3538–3547 Nucleic Acids Research, 2012, Vol. 40, No. 8 Published online 19 December 2011
doi:10.1093/nar/gkr1219

Genome-wide Runx2 occupancy in prostate cancer cells suggests a role in regulating secretion

Gillian H. Little[1,2,*], Houtan Noushmehr[3,4,5], Sanjeev K. Baniwal[2,6], Benjamin P. Berman[3,5], Gerhard A. Coetzee[3,4,7] and Baruch Frenkel[1,2,6,*]

[1]Departments of Biochemistry and Molecular Biology, [2]Institute of Genetic Medicine, [3]Preventive Medicine, [4]Norris Cancer Center, [5]USC Epigenome Center, [6]Orthopaedic Surgery and [7]Urology, Keck School of Medicine of the University of Southern California, Los Angeles, CA 90089, USA

Received October 13, 2011; Revised November 18, 2011; Accepted November 21, 2011

ABSTRACT

Runx2 is a metastatic transcription factor (TF) increasingly expressed during prostate cancer (PCa) progression. Using PCa cells conditionally expressing Runx2, we previously identified Runx2-regulated genes with known roles in epithelial–mesenchymal transition, invasiveness, angiogenesis, extracellular matrix proteolysis and osteolysis. To map Runx2-occupied regions (R2ORs) in PCa cells, we first analyzed regions predicted to bind Runx2 based on the expression data, and found that recruitment to sites upstream of the *KLK2* and *CSF2* genes was cyclical over time. Genome-wide ChIP-seq analysis at a time of maximum occupancy at these sites revealed 1603 high-confidence R2ORs, enriched with cognate motifs for RUNX, GATA and ETS TFs. The R2ORs were distributed with little regard to annotated transcription start sites (TSSs), mainly in introns and intergenic regions. Runx2-upregulated genes, however, displayed enrichment for R2ORs within 40 kb of their TSSs. The main annotated functions enriched in 98 Runx2-upregulated genes with nearby R2ORs were related to invasiveness and membrane trafficking/secretion. Indeed, using SDS–PAGE, mass spectrometry and western analyses, we show that Runx2 enhances secretion of several proteins, including fatty acid synthase and metastasis-associated laminins. Thus, combined analysis of Runx2's transcriptome and genomic occupancy in PCa cells lead to defining its novel role in regulating protein secretion.

INTRODUCTION

The mammalian Runx family includes three transcription factors that regulate cellular commitment and differentiation in several systems including hematopoeisis (Runx1), skeletogenesis (Runx2) and gastric epithelium development (Runx3) (1–4). Runx proteins also play positive and negative roles in carcinogenesis, with Runx2 emerging as a master regulator of tumor metastasis (5,6). The interest in its pro-metastatic activity initiated with the idea that expression of Runx2, an osteoblast master regulator (7,8), in prostate cancer (PCa) and breast cancer (BCa) cells could explain their high predilection to the skeleton (9). In fact, accumulative evidence now implicates Runx2 not only in bone targeting, but also in various other aspects of metastasis. Nuclear Runx2 is increased in malignant versus benign prostate tissue and is associated with tumor aggression in general and metastasis in particular (10,11). In animal models of carcinogenesis, increased Runx2 levels were observed early during the development of various malignancies, including PCa (12) and thyroid cancer (13). Mechanistically, Runx2 has been shown to promote epithelial–mesenchymal transition (EMT) and invasiveness, as well as survival in the bone environment (14,15). Thus, Runx2 plays a variety of roles during both early and late stages of cancer metastasis, including but not limited to bone metastasis.

Runx2 stimulates the expression of numerous genes with known roles in cancer metastasis (5,14–16). Among them are *SOX9*, *LCN2* and *SNAI2*, which promote EMT; *MMP9*, *MMP13* and *PGC* which play roles in extracellular matrix degradation and invasiveness; *VEGFA* and *EDN2*, which are important for angiogenesis; and *RANKL*, *PTHrP*, *IL8*, *SPHK1*, *EDG3* and *CSF2*, which likely contribute to the osteolytic phenotype induced by Runx2-expressing cancer cells that metastasize to bone (5,14). To gain a better understanding of Runx2's mechanisms in PCa, we performed Runx2 ChIP-seq analysis using C4-2B/Rx2^{dox} cells, in which Runx2 expression is inducible by doxycycline (14). Combined analysis of gene expression profiles and the genomic Runx2 occupancy data led to the identification of a subset of Runx2-responsive genes with nearby Runx2-occupied

*To whom correspondence should be addressed. Tel: +1 323 442 3914; Fax: +1 323 442 2764; Email: glittle@usc.edu
Correspondence may also be addressed to Baruch Frenkel. Email: frenkel@usc.edu

regions (R2ORs). These presumably direct target genes are related not only to cellular properties already associated with Runx2, such as invasiveness, but also to the secretory machinery, whose stimulation by Runx2 may facilitate cell–cell and cell–matrix interactions that promote metastasis.

MATERIALS AND METHODS

Cell culture

We previously described the cell lines C4-2B/Rx2^{dox}, LNCaP/Rx2^{dox} and MCF7/Rx2^{dox}, which express Flag-Runx2 in response to doxycycline (dox); C4-2B/Rx2-M^{dox}, which expresses a DNA-binding deficient mutant of Runx2 in response to dox; and T47D/shRx2^{dox}, which knocks down endogenous Runx2 in response to dox (14,15,17). C4-2B/Rx2^{dox}, C4-2B/Rx2-M^{dox}, LNCaP/Rx2^{dox} and T47D/shRx2^{dox} cells were maintained in RPMI medium and MCF7/Rx2^{dox} cells were maintained in DMEM, each supplemented with 10% FBS. Dox was added in fresh medium at 0.5 μg/ml.

Gene expression analysis

The GEO data set GSE24261, containing gene expression profiles of C4-2B/Rx2^{dox} cells treated in quadruplicate with dox or vehicle (14) was re-analyzed using statistical methods described previously (18). Briefly, differentially expressed genes were identified using Benjamini–Hochberg adjusted *t*-test comparing cells treated with dox or vehicle for either 1 or 2 days. To validate Runx2-responsiveness of individual genes of interest in independent cultures, RNA was isolated using the Bio-Rad Total RNA kit, and cDNA was made using Quanta qScript cDNA synthesis kit. qPCR was performed using a Bio-Rad CFX96 machine, Fermentas Maxima SYBR mastermix and the primers listed in Supplementary Table S1. Amplification reactions had efficiency of 90–110% and no primer-dimers were produced. Relative expression was calculated using the delta Ct method.

Chromatin immunoprecipitation-PCR

Flag-ChIP for Runx2 was carried out essentially as described for the androgen receptor (19) with the following modifications. C4-2B/Rx2^{dox} cultures containing 5×10^7 cells were crosslinked in 1.5% formaldehyde for 10 min at room temperature, and crosslinking was then halted by addition of glycine to 125 mM. Chromatin was sonicated to yield 500–1000 bp fragments in a buffer containing 50 mM Tris–HCl (pH 8.0), 0.1% SDS and 2 mM EDTA. Following preclearing with protein A dynabeads (Invitrogen), chromatin was incubated overnight with 0.5 μg Flag M2 antibody (Sigma) at +4°C and immunocomplexes were pulled down with Protein A dynabeads. Crosslinks for both ChIP and input DNA were reversed at 65°C for 5 h and DNA was cleaned using Qiagen QIAQuick spin DNA kit. Precipitated fragments were quantified by qPCR as described earlier, and percentage input values were corrected for negative control regions when indicated.

ChIP-sequencing and peak calling

Runx2 ChIP DNA along with ChIP input DNA were prepared as above from C4-2B/Rx2^{dox} cells treated with dox for 14 h, and high throughput sequencing of the 500–1000 bp fragments was performed using Illumina Hi-Seq 2000. Libraries for ChIP-seq were prepared following protocols recommended by Illumina. Enrichment for known target sequences was verified by qPCR before ChIP and input DNA were sequenced. A total of 98 165 959 and 92 795 549 sequences were generated for input and ChIP samples, respectively. MAQ (20) was used to generate 95 514 565 and 70 493 488 alignments to the hg18 reference genome. These alignments were reduced to 78 152 251 and 11 371 023 after filtering for only uniquely mapable positions in the genome (Mapping quality score $\geq$20) and condensing multiple reads aligned to identical positions in the genome (i.e. potential PCR duplicates) to a single count. Peak Calling was performed using FindPeaks 4.0 (21), with the ChIP input used as control. Briefly, using the filtered BAM alignment files for Runx2 and input, FindPeaks first searches for peaks in ChIP sample, then assesses each peak for enrichment relative to the Input control. It performs this by normalizing the two distributions globally using linear regression, and then modeling the background as a Poisson distribution about the regression line. Length of fragments was inferred using the FindPeaks 'triangle' distribution. Runx2 peaks with *P* values $<10^{-10}$ were identified as R2OR and used for downstream analyses. ChIP and input reads have been uploaded to the Sequence Read Archive, accession SRA048119.2 and to GEO, Accession GSE33889.

R2OR genomic distributions

Genomic distribution of R2ORs relative to gene annotations was performed using annotations from the UCSC knownGenes annotation track (hg18). For each annotation comparison, R2OR values were shown side by side with a set of regions picked randomly from the genome, with the randomized regions having the same number, distribution among different chromosomes and size as the actual R2ORs. One thousand such randomized sets were generated, and empirical background distributions were generated from this set of 1000 trials, from which summary statistics are shown in all comparisons.

Motif discovery and analysis

De novo motif discovery was performed using HOMER [script v3.1 (05-25-2011)] as previously described (22). Briefly, R2OR and background genomic sequences were extracted using Galaxy (23,24) and were divided into 'target' and 'background' sets for each application of the algorithm (HOMER perl script 'findMotifs.pl'). Motifs of length 6, 7, 8, 9, 10, 11 and 12 bp were identified separately for enrichment in 'target' compared to 'background' set using the cumulative hypergeometric distribution to score enrichment. To increase sensitivity of the method, up to two mismatches were allowed in each oligonucleotide sequence and distributions of CpG content in 'target' and 'background' sequences were selectively weighted to

equalize the distributions of CpG content in both sets. HOMER perl script 'annotatePeaks.pl' (22) and R software [R version 2.13.1, 2011-07-08, (25)] plus 'ggplot2' package (26) were used to generate genomic distribution of each identified motif. Additional statistical tools included the Database for Annotation, Visualization and Integrated Discovery (DAVID) and NextBio™. All statistical tests were done using R software [R version 2.13.1, 2011-07-08, (25)] and packages in Bioconductor (27).

Protein analyses

Western blot analysis was performed as previously described (14) with the following antibodies: Flag M2 from Sigma, GAPDH and FAS (h-300) from Santa Cruz Biotech, Laminin B1 (ab44941) and Laminin C1 (ab69632) from Abcam, LAMA5 (2F7) from Abnova and Tubulin from the Developmental Studies Hybridoma Bank. For mass spectrometry analysis of conditioned medium, C4-2B/Rx2^{dox} cells were treated with dox or vehicle for 48 h in complete growth media followed by 24 h in serum-free media. Non-adherent cells were removed from the culture supernatant by brief centrifugation, and proteins precipitated with 20% trichloroacetic acid were resolved by SDS–PAGE and stained with Coomassie Blue. Gel slices of interest were subjected to in-gel trypsin digestion as described (28). The resulting peptides were cleaned using C18 OmixTips (Varian) and analyzed by the Proteomics Facility at Childrens Hospital Los Angeles essentially as previously described (29) using an Eksigent nanoLC-2D coupled to a Thermo Orbitrap XL mass spectrometer. Proteins were identified from tandem mass spectra by comparison to the human Uniprot database (downloaded 200908) using complementary protein identification software systems, Bioworks 3.3.1 (Thermo) and Scaffold 3 (Proteome Software) (30). Protein identification was based on at least two peptides, with peptide and protein probabilities of at least 95%.

RESULTS

Runx2 binds its targets in a cyclical fashion

Unlike most PCa tumors, the LNCaP and C4-2B cell lines are essentially Runx2-negative, providing a close-to-zero background system for the investigation of Runx2 function in PCa. In C4-2B/Rx2^{dox} and LNCaP/Rx2^{dox} cells, Flag-Runx2 is expressed in response to dox at levels comparable to or lower than those seen in other PCa cells and osteoblasts (14). Prior to performing Runx2 ChIP-seq in C4-2B/Rx2^{dox} cells, and because there are relatively few published studies of Runx2 ChIP in general and in PCa cells in particular, we first optimized our ChIP assay based on Runx2 occupancy upstream of the *CSF2* and *KLK2* genes (Figure 1A). We chose these regions because *CSF2* and *KLK2* were strongly stimulated by Runx2 in C4-2B/Rx2^{dox} cells (14), and because they contained clusters of Runx motifs (Figure 1A), a feature thought to constitute strong binding sites for Runx transcription factors (31,32). Runx2 binding upstream of the *CSF2* and *KLK2* genes was tested by quantitative ChIP assays every 2 h between 12 and 24 h of Runx2 induction. A cyclical binding pattern of Runx2 was obvious (Figure 1B), even though the protein level of Runx2 did not change significantly (Figure 1C). Untreated C4-2B/Rx2^{dox} cells were processed in parallel; because they do not express Flag-Runx2, they serve as an ideal negative control for our ChIP experiments. As shown in Figure 1B, Flag-ChIP of the untreated cells did not show any enrichment at the *CSF2* and *KLK2* versus the negative control regions, indicating high specificity of the Flag-ChIP assay.

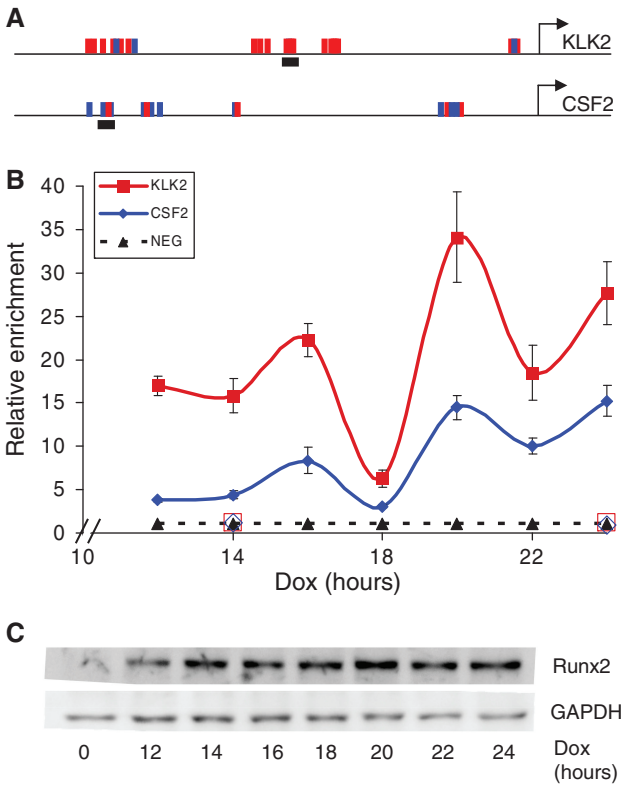

Figure 1. Cyclical genomic recruitment of Runx2 to *KLK2* and *CSF2*. (**A**) Diagram depicting predicted Runx binding sites within the 5-kb sequences upstream of the *KLK2* and *CSF2* TSSs. Runx motifs that appear as clusters are shown, with red and blue tics representing consensus binding sites with high (>9) and medium scores (<9, >6), respectively, according to the Runx1 matrix from JASPAR. Horizontal bars indicate the areas targeted for Runx2 ChIP-qPCR analysis. (**B**) Runx2 ChIP-qPCR time course analysis for binding to the Runx motifs upstream of the *KLK2* (red) and *CSF2* TSSs (blue). C4-2B/Rx2^{dox} cells were fed fresh medium without (open boxes) or with 0.5 μg/ml dox (closed boxes) and harvested at the indicated time points for ChIP assay using anti-Flag antibodies. Data points (mean ± SEM; $n = 3$) depict enrichment values corrected for the average of two negative control regions (triangles, dashed line). The raw values for the *KLK2* and *CSF2* Runx2 ChIPs oscillated within the 0.15–0.28% and the 0.04–0.16% input range, respectively, compared to 0.006–0.030% input for the negative control regions and the ChIPs obtained without FLAG-Runx2 induction. Results shown are representative of three independent experiments using separate chromatin preparations. (**C**) Western blot analysis of Flag-Runx2 in cells treated in parallel to those used in B, with GAPDH serving as a loading control.

Runx2 primarily occupies intergenic and intronic regions, distal to TSSs

For genome-wide mapping of R2ORs, Illumina high throughput single end sequencing was performed on a large-scale Runx2 ChIP, in which the *CSF2* and *KLK2* upstream Runx motifs were enriched by 8- and 16.5-fold, respectively. High throughput sequencing resulted in approximately 11 million sequence tags that uniquely mapped to the human genome build 18. As a control, the input DNA material was also subjected to high throughput sequencing, resulting in 78 million tags that were uniquely mapped. We initially examined the ChIP-seq data for Runx2 occupancy at the *KLK2* and *CSF2* loci (Figure 2A). In both cases, several R2ORs were readily identified, some with more occupancy than the regions initially selected for the conventional ChIP assays (black bars in Figures 1A and 2A). At both loci, Runx2 occupancy occurred at presumed enhancer elements as well as at the transcription start sites (TSSs).

Using the FindPeaks program (21), we identified in the C4-2B cell genome 5413 R2ORs with an FDR-adjusted *P*-value <0.01 (Supplementary Table S2). Among them, some were found in the vicinity of genes previously shown to be regulated by Runx2 in PCa and other cell types, including *CXCL12*, *MMP9*, *VEGFA* and *DUSP1* (14), *PLAC8* and *CRISPLD2* (15), *HEY1* and *TNC* (33) as well as *RUNX1*, *RUNX3* and *RUNX2* itself (Supplementary Figure S1). Runx2 occupancy at rRNA genes (34) could not be assessed because these gene sequences are highly repetitive and thus not unequivocally mapped to the hg18 human genome build used in our study.

For further analyses, we applied a more stringent FDR-adjusted *P*-value of 10^{-10} resulting in 1603 peaks that included *KLK2*, but not *CSF2* R2ORs (Supplementary Table S3). We then tested biological reproducibility of Runx2 occupancy at 16 regions by quantitative PCR (qPCR) of independent chromatin immunoprecipitates. Occupancy was confirmed in every case (Supplementary Figure S2A). Furthermore, when plotted against peak scores, the qPCR values were in good agreement with the ChIP-seq data (Figure 2B). In addition to the validation of Runx2 ChIP-seq peaks in C4-2B/Rx2^{dox} cells, we analyzed in a similar fashion the related LNCaP/Rx2^{dox} PCa cell line (14) and observed Runx2 occupancy at all 16 sites (Supplementary Figure S2B). Finally, the specificity of our results was tested by measuring occupancy of 10 R2ORs by a DNA-binding incompetent Runx2 mutant (14). Flag-ChIP assays of C4-2B/Rx2-M^{dox} cells, which inducibly express the Flag-tagged Runx2 mutant, showed that in contrast to wild-type Runx2, the mutant form did not bind to any of the R2ORs (Supplementary Figure S2C).

Next we assessed the distribution of the 1603 stringently defined R2ORs in relation to RefSeq gene annotations. As shown in Figure 2C, the distribution of R2ORs with respect to nearest TSSs is very similar to the distribution of matched random sets of genomic sequences, with R2ORs having a slight preference for TSSs. The vast majority of R2ORs are located in introns (44%) and distal intergenic regions (50%) with only 2% at promoters (Figure 2D). Thus, similar to Runx1 in differentiating megakaryocytes (35) and in hematopoietic progenitor cells (36), Runx2 in PCa cells appears to primarily associate with enhancers and not promoters.

Motif analysis

The three mammalian RUNX proteins have highly homologous DNA-binding domains and therefore bind similar consensus TGTGGT motifs *in vitro*. *De novo* motif-finding analysis of the 1603 top R2ORs in C4-2B/Rx2^{dox} cells revealed the highest enrichment for the YTGTGGTTW sequence, containing the TGTGGT consensus as a core (Figure 3A). Eighty-one percent of the R2ORs in C4-2B/Rx2^{dox} cells contained this sequence (Figure 3C), which is similar to that found for Runx1 in hematopoietic cells (35–37) (Figure 3A). Following the remarkable but expected enrichment of the R2ORs for the classical Runx motif ($P = 10^{-699}$), additional *de novo* motif analysis indicated strong enrichment ($P < 10e^{-100}$) for the GATA consensus motif, AGATAA, as well as a motif representing a hybrid of Runx and Ets cognate sequences (Figure 3B). The GATA and the Runx/Ets motifs were found in 26% and 6% of R2ORs, respectively (Figure 3C). Both GATA and ETS transcription factors have been previously reported to physically interact with RUNX proteins (35–42).

Runx2-induced genes with nearby R2ORs are functionally related to protein secretion

Although R2ORs are generally far from TSSs, we asked whether they were specifically enriched near TSSs of Runx2-responsive genes. We first re-analyzed our genome-wide expression data (14) and generated four sets of genes, those up- or down-regulated after 1 or 2 days of Runx2 induction (FDR-adjusted $P < 10^{-3}$; Supplementary Figure S3). For each gene set, we plotted the histogram of distances between the responsive TSSs and the nearest R2ORs (Figure 4 and Supplementary Figure S4). To control for the responsive TSSs, we generated multiple random size-matched sets of TSSs, and subjected them to the same analysis. A remarkable enrichment for R2ORs was observed within ~40 kb of the TSSs of upregulated, but not downregulated, genes (Figure 4 and Supplementary Figure S4). Supplementary Table S4 lists 98 upregulated genes with nearby (<40 kb) R2ORs, presumably direct Runx2 targets.

To ascertain the functional significance of the 98 Runx2-upregulated genes with nearby R2ORs, we carried out pathway analysis using DAVID (43). The top functional pathways enriched in this gene set related to cell attachment and invasion functions (Supplementary Table S5), consistent with the established role of Runx2 in metastasis (5,14,16). In addition, DAVID analysis of the 98-gene set highlighted membrane trafficking and secretion as a potential Runx2 target pathway (Figure 5A and Supplementary Table S5). In particular, Runx2-upregulated genes with nearby R2ORs coded for enzymes that modify membrane lipids and small GTPases of the Rab family, major components of the

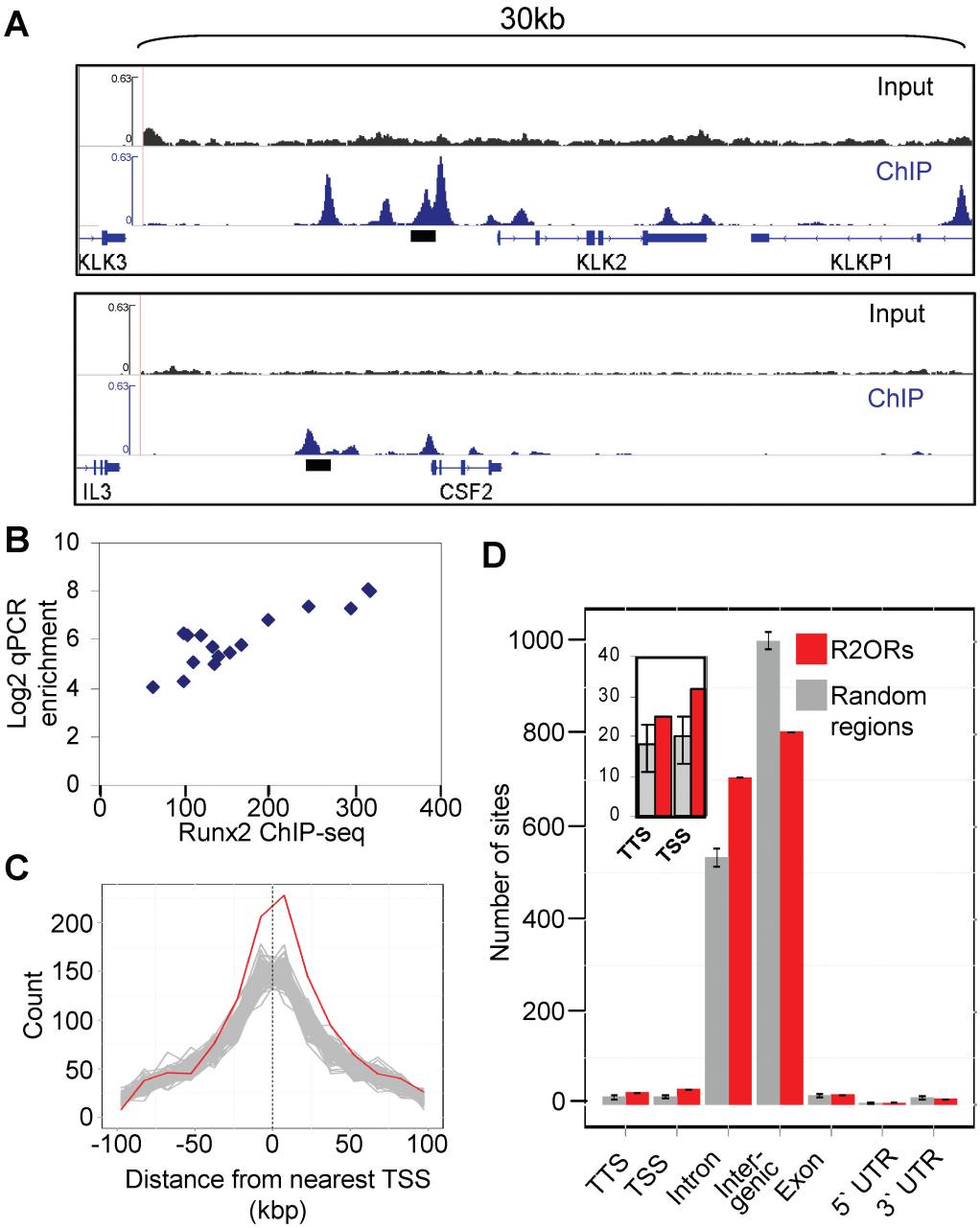

Figure 2. Genome-wide characterization of Runx2 occupied regions (R2ORs). C4-2B/Rx2^{dox} cells were subjected to Runx2 ChIP-seq analysis after dox treatment and immunoprecipitation of Runx2-bound DNA fragments with anti-FLAG antibodies. (**A**) ChIP-seq results showing R2ORs upstream of the *KLK* and CSF2 TSS*s*. Raw ChIP-seq data are presented as frequency of reads per location for 30 kb of DNA sequences at the *KLK2* (top) and *CSF2* (bottom) loci. For each locus, the upper track shows results for chromatin aliquoted prior to immunoprecipitation (input). Regions investigated in Figure 1 by conventional ChIP assays are marked by black bars. (**B**) Sixteen Runx2 ChIP-seq peaks were validated by conventional ChIP-qPCR and the ChIP-seq scores are plotted against the qPCR enrichment factors. (**C**) Distance from the 1603 top R2ORs to the nearest TSS were mapped (red) and are shown along with control distribution patterns of 1000 sets of 1603 matched random sequences (gray). *Y*-axis values are numbers of R2ORs per 15 kb window. (**D**) Genomic distribution of the 1603 top R2ORs (red bars) versus that of 1000 sets of matched random sequences (gray bars; mean ± SD). *TSS* refers to −1000 to +100 bp from 5′-end of annotated RNA. Transcription Termination Site (*TTS*) is defined as −100 to +1000 bp from the 3′-end of the transcript. *Inset* shows blow up of TTS and TTS data.

secretory pathway (Figure 5A) (44–47). ChIP-seq results showing R2ORs near the TSSs of *RAB3B*, *RAB43* and *RAB35* are presented in Figure 5B. Validation of these R2ORs in independent ChIP experiments, as well as independent validation of Runx2-mediated upregulation of *RAB3B*, *RAB43* and *RAB35* mRNA are presented in Figure 5C and D, respectively.

Based on the results of the integrated analysis of Runx2 occupancy and the Runx2 transcriptome, we next asked whether Runx2 regulated protein secretion by cancer cells. C4-2B/Rx2^{dox} cells were treated with either vehicle as control or dox to induce Runx2, and proteins in conditioned media were visualized by SDS–PAGE and Coomassie Blue staining. Compared to control cultures,

conditioned medium from cells expressing Runx2 exhibited dramatically increased levels of several secreted proteins (Figure 6A). The influence of Runx2 on protein secretion was also tested in breast cancer cells. As shown in Supplementary Figure S5, Runx2 expression enhanced protein secretion by the breast cancer cell line MCF7/Rx2^{dox}; and, Runx2 knock-down in the Runx2-positive T47D cell line inhibited protein secretion. Thus, Runx2 appears to induce a secretory phenotype in both prostate and breast cancer cells, potentially contributing to its pro-metastatic property.

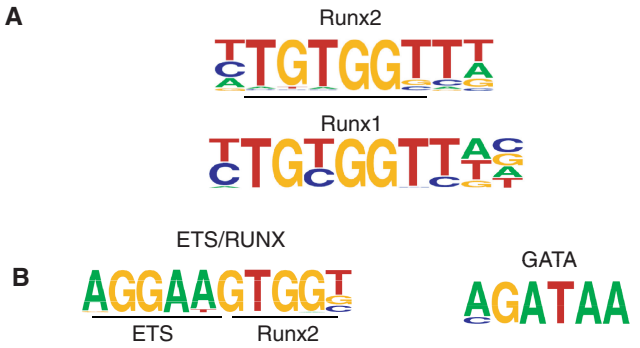

C

	percentage		motifs /	
	R2OR	Background	R2OR	*p*value
Runx2	80.8	16.5	1.62	1e-699
ETS/RUNX2	5.9	0.2	1.06	1e-133
GATA	25.6	7.7	1.22	1e-103

Figure 3. DNA sequence motifs enriched in R2ORs. Motifs enriched in R2ORs compared to 1603 matched random sequences were identified using HOMER 3.1. (**A**) Logo for the top motif (*Runx2*) is shown above the Runx1 logo identified by Pencovich *et al.* (35). (**B**) Motifs identified after R2ORs were re-analyzed as in A following masking of the Runx2 motifs. (**C**) Motif statistics. *P*-values are for motif enrichment. The percentages of R2ORs containing at least one copy of each motif are indicated against the percentage of motif-containing random sequences. *Motifs/R2OR* indicates for each motif the average number of copies per R2OR in R2ORs containing at least one copy.

Runx2 particularly augmented the secretion of high molecular weight proteins (Figure 6A). To identify some of them, we analyzed by mass spectrometry proteins with MW >120 kDa present in medium conditioned by dox-treated C4-2B/Rx2^{dox} cultures (bracket in Figure 6A). Sixteen proteins were identified with 95% confidence (Supplementary Table S6). Of the respective mRNAs, only three were upregulated by Runx2 (Supplementary Table S6), and among the remaining 13 proteins, 4 of particular interest were subjected to western blot analysis. As shown in Figure 6B, fatty acid synthase (FAS), which is abundantly expressed by PCa cells and serves as a serum marker for cancer progression (48–50), was readily detectable in medium conditioned by Runx2-expressing C4-2B cells, but not in control conditioned medium. Because FAS levels were comparable between the respective cell extracts (Figure 6B), we conclude that Runx2 stimulated FAS secretion. More interestingly, the 16 proteins identified by mass spectrometry included the laminins α5 (LAMA5), β1 (LAMB1) and γ1 (LAMC1), which together constitute the laminin 511 heterotrimer, strongly implicated in cancer cell motility (51). Of these three laminins, Runx2 robustly stimulated the secretion of LAMA5 and LAMB1 while having no or little effect on the respective cellular protein levels (Figure 6B). Because LAMC1 was equally present in media from dox-treated and control cultures (Figure 6B), the data suggest that Runx2-mediated LAMA5 and LAMB1 secretion may facilitate the assembly of the metastatic laminin 511 in prostate cancer cells. In summary, bioinformatics analysis of Runx2 target genes with nearby R2ORs suggested a role in regulating protein secretion, and such a role was indeed demonstrated for

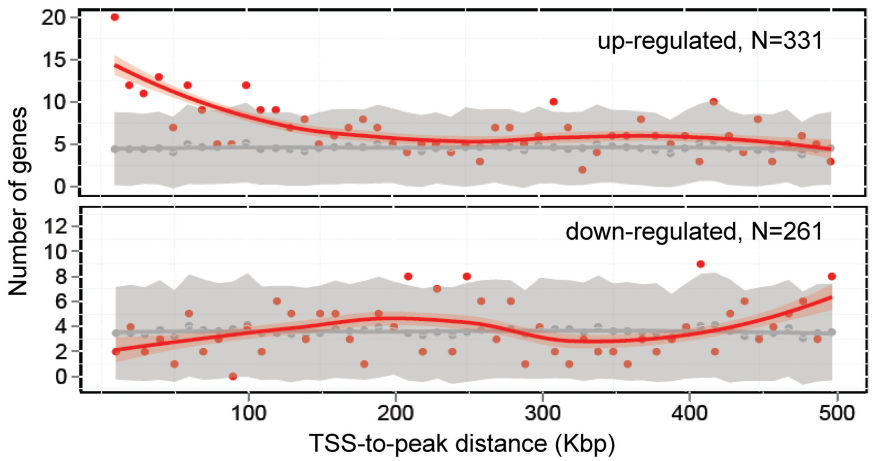

Figure 4. R2ORs are enriched close to TSS of upregulated genes. Analysis of the distances between the TSSs of differentially expressed genes and their respective nearest R2ORs was performed for genes whose expression changed after 24 h of Runx2 induction (Supplementary Figure S3). The distances were assigned to 10 kb windows, and the number of genes in each window (red dots) was plotted for the up (top) and down (bottom)-regulated genes. One thousand size-matched random gene sets were analyzed in a similar fashion to generate the background control (gray). Lines are best-fit curves and shaded areas represent 95% confidence levels for the lines. Note that R2ORs are enriched near TSSs of upregulated genes. Similar results were obtained for genes whose expression changed after 48 h of Runx2 induction (Supplementary Figure S4).

A

Term	Genes	PValue	Fold Enrichment
IPR004299:Membrane bound O-acyl transferase, MBOAT	DGAT1, MBOAT7, LPCAT3	0.002	47.33
GO:0005905~coated pit	SH3BP4, RAB35, AP2S1	0.025	11.94
IPR003579:Ras small GTPase, Rab type	RAB3B, RAB43, RAB35	0.047	8.53
GO:0030136~clathrin-coated vesicle	SH3BP4, RAB3B, RAB35, AP2S1	0.038	5.31

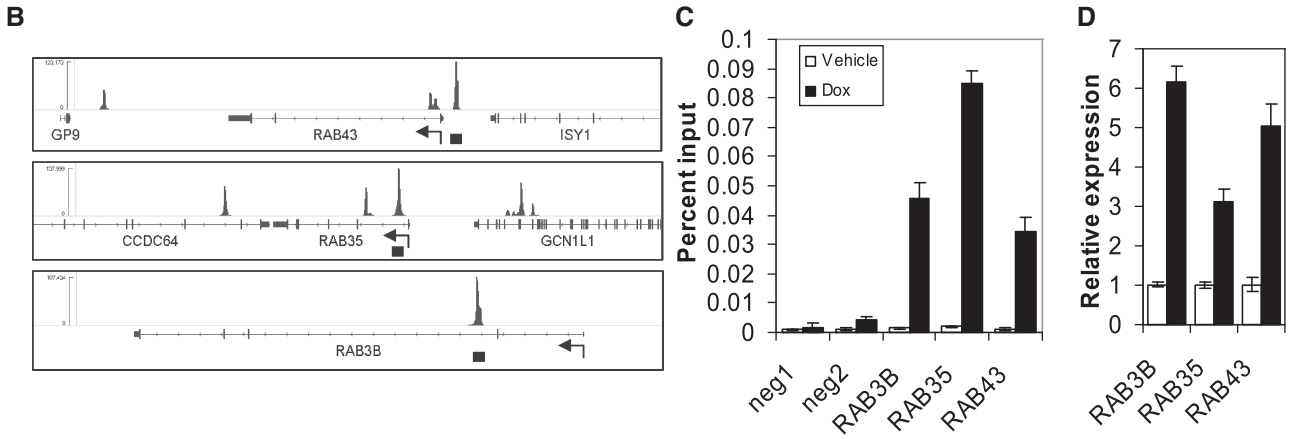

Figure 5. Evidence that Runx2 directly stimulates genes associated with membrane trafficking and secretion. (**A**) The 98 Runx2-upregulated genes with nearby R2ORs were analyzed using DAVID for functional annotation. Top functions with fold enrichment >5 and $P < 0.05$ are listed in Supplementary Table S5, and those related to membrane trafficking and secretion are listed in *A*, along with the specific Runx2-stimulated genes in each functional category. (**B**) ChIP-seq results showing R2ORs near the TSSs (arrows) of three Rab genes. (**C**) ChIP-qPCR validation of R2ORs indicated in B by black bars. (**D**) RT-qPCR analysis of the effects of Runx2 on the mRNA expression of *RAB3B*, *RAB35* and *RAB43*. Primers used in C and D are listed in Supplementary Table 1 (mean ± SEM; $n = 3$).

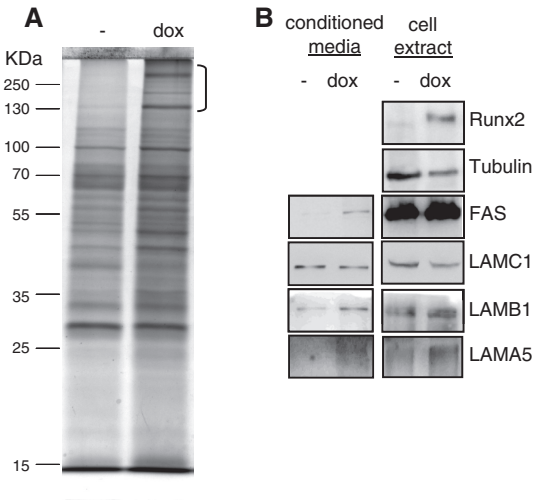

Figure 6. Runx2 increases protein secretion by PCa cells. (**A**) Proteins were precipitated from media conditioned by dox-treated and control C4-2B/Rx2^{dox} cells, resolved in SDS–PAGE and stained by Coomassie Blue. Proteins in the region indicated by a bracket were analyzed by mass spectrometry and those identified with >95% confidence are listed in Supplementary Table S6. (**B**) Western blot analysis of the indicated proteins in conditioned media or whole cell extracts from control and dox-treated C4-2B/Rx2^{dox} cultures.

several proteins, thus providing novel insight into the pro-metastatic property of Runx2.

DISCUSSION

Runx2 regulates many genes and pathways promoting metastatic properties such as invasiveness, extravasation, angiogenesis, osteolysis and drug resistance (5,14,52). The present study demonstrates a role for Runx2 in regulating protein secretion by PCa cells (Figure 6). The hypothesis that Runx2 regulates secretion was based on the association of this cellular function with a set of 98 Runx2-stimulated genes with nearby Runx2-occupied regions (R2ORs). Such hypothesis was not invoked when the Runx2 transcriptome was originally analyzed by Ingenuity Pathway Analysis (14), or when re-analyzed in this study by DAVID without regard to R2ORs (Supplementary Table S7). Interestingly, the association of Runx2-regulated genes with R2ORs was found for up- but not down-regulated genes (Figure 4 and Supplementary Figure S4). Lack of R2OR enrichment near Runx2-downregulated genes suggests that their inhibition by Runx2 is likely a secondary event.

Our ChIP-seq results for Runx2 in PCa cells share many features with those described for Runx1 in megakaryocytes and in hematopoietic progenitor cells (35,36). Both transcription factors bind mostly at regions far from gene promoters, likely enhancers that form shortcut loops to contact distant TSSs, up to hundreds of kilo-bases away. Whereas extraordinary efforts are needed to map such long-range interactions between enhancers and promoters, shorter-range interactions are suggested by the excess of R2ORs within 40 kb of TSSs of Runx2-upregulated genes. Such shorter-range interactions may be preferentially utilized by Runx2 in PCa cells to execute defined biological functions such as cell motility and protein secretion (Supplementary Table S5). It will be interesting to know if Runx1-upregulated genes with nearby Runx1-occupied regions (R1ORs) execute defined

biological functions in hematopoietic progenitor cells or in megakaryocytes (35,36). Additional similarities between the Runx2 and the Runx1 ChIP-seq results relate to the DNA motifs enriched within the respective occupied regions. The motif most significantly enriched in R2ORs, YTGTGGTTW, is almost identical to that found in R1ORs in hematopoietic cells (35). Finally, both the R1ORs and the R2ORs were enriched for GATA and ETS factors, indeed both also show evidence of a Runx/Ets hybrid motif (37).

Using the dox-inducible system for Runx2 expression, we observed cyclical genomic occupancy of Runx2 (Figure 1B). It remains to be seen whether such behavior, which has been observed for ligand-activated transcription factors such as the estrogen receptor (53,54), is shared by Runx1, Runx3 or other TFs not activated by ligand. It will also be interesting to know whether the composition of Runx2-containing complexes changes between cycles of occupancy. Be that as it may, the robustness of the ChIP-seq peaks (Figures 1A and 5B) is attributable in part to synchronization of Runx2 binding after dox treatment, as well as the Flag-ChIP-seq approach that mitigated the requirement for high quality antibodies against Runx2 (55–58).

Runx2 stimulated the secretion of many proteins by PCa cells, among which were the laminins α5 and ß1. Because laminin γ1 is also secreted by C4-2B/Rx2^{dox} cells, the data suggest that Runx2 may render prostate cancer cells able to synthesize the α5β1γ1 laminin heterotrimer, also known as 511. Laminin 511 is abundant in malignant tumors, blood vessels and bone and has been implicated in guiding cancer cell metastasis as well as promoting aggression of breast, prostate and other cancer cells through activation of integrin signaling (51,59–63). Interestingly, integrin signaling is also enriched in the 98 upregulated genes with nearby R2ORs (Supplementary Table S5). Thus, via direct target genes, Runx2 may manipulate the cell microenvironment through the secretion of laminins, while augmenting cellular response through expression of the respective membrane signaling proteins.

In conclusion, Runx2 occupies sites in the PCa cell genome that are enriched for the canonical TGTGGT-containing Runx consensus motif and are usually located far from TSSs of annotated genes. A set of presumably direct Runx2-upregulated genes was identified based on proximity to R2ORs. These genes likely mediate both known and novel metastatic properties of Runx2, namely, cell motility and protein secretion.

SUPPLEMENTARY DATA

Supplementary Data are available at NAR Online: Supplementary Tables 1–7 and Supplementary Figures 1–5.

ACKNOWLEDGEMENTS

The authors are thankful to Charles Nicolet at the USC Epigenome Center for high throughput sequencing; to the USC High Performance Computing Center (http://www.usc.edu/hpcc/) for high performance computing support; and to Susan Lee at the Proteomics Facility of USC/Childrens Hospital Los Angeles for identification of proteins in conditioned media.

FUNDING

National Institutes of Health (NIH) (DK07112 to B.F. and CA109147 to G.A.C.). H.N. is supported by NIH training grant 5T32CA009320-27. B.F. holds the J. Harold and Edna L. LaBriola Chair in Genetic Orthopedic Research at USC. Funding for open access charge: NIH DK07112.

Conflict of interest statement. None declared.

REFERENCES

1. Komori,T., Yagi,H., Nomura,S., Yamaguchi,A., Sasaki,K., Deguchi,K., Shimizu,Y., Bronson,R.T., Gao,Y.H., Inada,M. *et al.* (1997) Targeted disruption of Cbfa1 results in a complete lack of bone formation owing to maturational arrest of osteoblasts. *Cell*, **89**, 755–764.
2. Otto,F., Thornell,A.P., Crompton,T., Denzel,A., Gilmour,K.C., Rosewell,I.R., Stamp,G.W.H., Beddington,R.S.P., Mundlos,S., Olsen,B.R. *et al.* (1997) Cbfa1, a candidate gene for cleidocranial dysplasia syndrome, is essential for osteoblast differentiation and bone development. *Cell*, **89**, 765–771.
3. Li,Q.-L., Ito,K., Sakakura,C., Fukamachi,H., Inoue,K.-i., Chi,X.-Z., Lee,K.-Y., Nomura,S., Lee,C.-W., Han,S.-B. *et al.* (2002) Causal relationship between the loss of RUNX3 expression and gastric cancer. *Cell*, **109**, 113–124.
4. Okuda,T., van Deursen,J., Hiebert,S.W., Grosveld,G. and Downing,J.R. (1996) AML1, the target of multiple chromosomal translocations in human leukemia, is essential for normal fetal liver hematopoiesis. *Cell*, **84**, 321–330.
5. Pratap,J., Lian,J.B. and Stein,G.S. (2011) Metastatic bone disease: role of transcription factors and future targets. *Bone*, **48**, 30–36.
6. Blyth,K., Vaillant,F., Jenkins,A., McDonald,L., Pringle,M.A., Huser,C., Stein,T., Neil,J. and Cameron,E.R. (2010) Runx2 in normal tissues and cancer cells: a developing story. *Blood Cells Mol. Dis.*, **45**, 117–123.
7. Ducy,P., Zhang,R., Geoffroy,V., Ridall,A.L. and Karsenty,G. (1997) Osf2/Cbfa1: a transcriptional activator of osteoblast differentiation. *Cell*, **89**, 747–754.
8. Banerjee,C., McCabe,L.R., Choi,J.Y., Hiebert,S.W., Stein,J.L., Stein,G.S. and Lian,J.B. (1997) Runt homology domain proteins in osteoblast differentiation: AML3/CBFA1 is a major component of a bone-specific complex. *J. Cell. Biochem.*, **66**, 1–8.
9. Koeneman,K.S., Yeung,F. and Chung,L.W.K. (1999) Osteomimetic properties of prostate cancer cells: a hypothesis supporting the predilection of prostate cancer metastasis and growth in the bone environment. *Prostate*, **39**, 246–261.
10. Chua,C.-W., Chiu,Y.-T., Yuen,H.-F., Chan,K.-W., Man,K., Wang,X., Ling,M.-T. and Wong,Y.-C. (2009) Suppression of androgen-independent prostate cancer cell aggressiveness by FTY720: validating Runx2 as a potential antimetastatic drug screening platform. *Clin. Cancer Res.*, **15**, 4322–4335.
11. Onodera,Y., Miki,Y., Suzuki,T., Takagi,K., Akahira,J.-i., Sakyu,T., Watanabe,M., Inoue,S., Ishida,T., Ohuchi,N. *et al.* (2010) Runx2 in human breast carcinoma: its potential roles in cancer progression. *Cancer Sci.*, **101**, 2670–2675.
12. Lim,M., Zhong,C., Yang,S., Bell,A.M., Cohen,M.B. and Roy-Burman,P. (2010) Runx2 regulates survivin expression in prostate cancer cells. *Lab. Investig.*, **90**, 222–233.
13. Vasko,V., Espinosa,A.V., Scouten,W., He,H., Auer,H., Liyanarachchi,S., Larin,A., Savchenko,V., Francis,G.L., de la Chapelle,A. *et al.* (2007) Gene expression and functional evidence of epithelial-to-mesenchymal transition in papillary

thyroid carcinoma invasion. *Proc. Natl Acad. Sci.*, **104**, 2803–2808.
14. Baniwal,S.K., Khalid,O., Gabet,Y., Shah,R.R., Purcell,D.J., Mav,D., Kohn-Gabet,A.E., Shi,Y., Coetzee,G.A. and Frenkel,B. (2010) Runx2 transcriptome of prostate cancer cells: insights into invasiveness and bone metastasis. *Mol. Cancer*, **9**, 258.
15. Chimge,N.-O., Baniwal,S.K., Little,G.H., Chen,Y.-b., Kahn,M., Tripathy,D., Borok,Z. and Frenkel,B. (2011) Regulation of Breast Cancer Metastasis by Runx2 and Estrogen Signaling: Role of SNAI2. *Breast Cancer Research*, **13**, R127.
16. Akech,J., Wixted,J.J., Bedard,K., van der Deen,M., Hussain,S., Guise,T.A., van Wijnen,A.J., Stein,J.L., Languino,L.R., Altieri,D.C. *et al.* (2010) Runx2 association with progression of prostate cancer in patients: mechanisms mediating bone osteolysis and osteoblastic metastatic lesions. *Oncogene*, **29**, 811–821.
17. Baniwal,S.K., Little,G.H., Chimge,N.-O. and Frenkel,B. (2012) Runx2 controls a feed-forward loop between androgen and prolactin-induced protein (PIP) in stimulating T47D cell proliferation. *J. Cell. Physiol*, **227**, 2276–2282.
18. Noushmehr,H., Weisenberger,D.J., Diefes,K., Phillips,H.S., Pujara,K., Berman,B.P., Pan,F., Pelloski,C.E., Sulman,E.P., Bhat,K.P. *et al.* (2010) Identification of a CpG island methylator phenotype that defines a distinct subgroup of glioma. *Cancer Cell*, **17**, 510–522.
19. Jia,L., Berman,B.P., Jariwala,U., Yan,X., Cogan,J.P., Walters,A., Chen,T., Buchanan,G., Frenkel,B. and Coetzee,G.A. (2008) Genomic androgen receptor-occupied regions with different functions, defined by histone acetylation, coregulators and transcriptional capacity. *PLoS ONE*, **3**, e3645.
20. Li,H., Ruan,J. and Durbin,R. (2008) Mapping short DNA sequencing reads and calling variants using mapping quality scores. *Genome Res.*, **18**, 1851–1858.
21. Fejes,A.P., Robertson,G., Bilenky,M., Varhol,R., Bainbridge,M. and Jones,S.J.M. (2008) FindPeaks 3.1: a tool for identifying areas of enrichment from massively parallel short-read sequencing technology. *Bioinformatics*, **24**, 1729–1730.
22. Heinz,S., Benner,C., Spann,N., Bertolino,E., Lin,Y.C., Laslo,P., Cheng,J.X., Murre,C., Singh,H. and Glass,C.K. (2010) Simple combinations of lineage-determining transcription factors prime cis-regulatory elements required for macrophage and B cell identities. *Mol. Cell*, **38**, 576–589.
23. Goecks,J., Nekrutenko,A. and Taylor,J. (2011) Galaxy: a comprehensive approach for supporting accessible, reproducible, and transparent computational research in the life sciences. *Genome Biol.*, **11**, R86.
24. Blankenberg,D., Kuster,G.V., Coraor,N., Ananda,G., Lazarus,R., Mangan,M., Nekrutenko,A. and Taylor,J. (2010) *Current Protocols in Molecular Biology*, Chapter 19. John Wiley & Sons, Inc., pp. Unit 19.10.11–21.
25. Team,R.D.C. (2008) *R: A language and environment for statistical computing*. R Foundation for Statistical Computing, Vienna, Austria.
26. Wickham,H. (2009) *ggplot2: Elegant Graphics for Data Analysis*. Springer, New York.
27. Gentleman,R.C., Carey,V.J., Bates,D.M., Bolstad,B., Dettling,M., Dudoit,S., Ellis,B., Gautier,L., Ge,Y., Gentry,J. *et al.* (2004) Bioconductor: open software development for computational biology and bioinformatics. *Genome Biol.*, **5**, R80.
28. Shevchenko,A., Tomas,H., Havlis,J., Olsen,J.V. and Mann,M. (2007) In-gel digestion for mass spectrometric characterization of proteins and proteomes. *Nat. Protoc.*, **1**, 2856–2860.
29. Berndsen,C.E., Tsubota,T., Lindner,S.E., Lee,S., Holton,J.M., Kaufman,P.D., Keck,J.L. and Denu,J.M. (2008) Molecular functions of the histone acetyltransferase chaperone complex Rtt109-Vps75. *Nat. Struct. Mol. Biol.*, **15**, 948–956.
30. Sadygov,R.G., Cociorva,D. and Yates,J.R. (2004) Large-scale database searching using tandem mass spectra: looking up the answer in the back of the book. *Nat. Methods*, **1**, 195–202.
31. Ji,C., Casinghino,S., Chang,D.J., Chen,Y., Javed,A., Ito,Y., Hiebert,S.W., Lian,J.B., Stein,G.S., McCarthy,T.L. *et al.* (1998) CBFa(AML/PEBP2)-related elements in the TGF-β type I receptor promoter and expression with osteoblast differentiation. *J. Cell. Biochem.*, **69**, 353–363.
32. Javed,A., Gutierrez,S., Montecino,M., van Wijnen,A.J., Stein,J.L., Stein,G.S. and Lian,J.B. (1999) Multiple Cbfa/AML sites in the rat osteocalcin promoter are required for basal and vitamin D-responsive transcription and contribute to chromatin organization. *Mol. Cell. Biol.*, **19**, 7491–7500.
33. Baniwal,S., Shah,P., Shi,Y., Haduong,J., DeClerck,Y., Gabet,Y. and Frenkel,B. (2011) Runx2 promotes both osteoblastogenesis and novel osteoclastogenic signals in ST2 mesenchymal progenitor cells. *Osteoporos. Int.*, **23**, 1399–1413.
34. Young,D.W., Hassan,M.Q., Pratap,J., Galindo,M., Zaidi,S.K., Lee,S.-H., Yang,X., Xie,R., Javed,A., Underwood,J.M. *et al.* (2007) Mitotic occupancy and lineage-specific transcriptional control of rRNA genes by Runx2. *Nature*, **445**, 442–446.
35. Pencovich,N., Jaschek,R., Tanay,A. and Groner,Y. (2011) Dynamic combinatorial interactions of RUNX1 and cooperating partners regulates megakaryocytic differentiation in cell line models. *Blood*, **117**, e1–e14.
36. Wilson,N.K., Foster,S.D., Wang,X., Knezevic,K., Schütte,J., Kaimakis,P., Chilarska,P.M., Kinston,S., Ouwehand,W.H., Dzierzak,E. *et al.* (2010) Combinatorial transcriptional control in blood stem/progenitor cells: genome-wide analysis of ten major transcriptional regulators. *Cell Stem Cell*, **7**, 532–544.
37. Hollenhorst,P.C., Chandler,K.J., Poulsen,R.L., Johnson,W.E., Speck,N.A. and Graves,B.J. (2009) DNA specificity determinants associate with distinct transcription factor functions. *PLoS Genet.*, **5**, e1000778.
38. Kim,W.-Y., Sieweke,M., Ogawa,E., Wee,H.-J., Englmeier,U., Graf,T. and Ito,Y. (1999) Mutual activation of Ets-1 and AML1 DNA binding by direct interaction of their autoinhibitory domains. *EMBO J.*, **18**, 1609–1620.
39. Waltzer,L., Ferjoux,G., Bataille,L. and Haenlin,M. (2003) Cooperation between the GATA and RUNX factors Serpent and Lozenge during *Drosophila hematopoiesis*. *EMBO J.*, **22**, 6516–6525.
40. Elagib,K.E., Racke,F.K., Mogass,M., Khetawat,R., Delehanty,L.L. and Goldfarb,A.N. (2003) RUNX1 and GATA-1 coexpression and cooperation in megakaryocytic differentiation. *Blood*, **101**, 4333–4341.
41. Fowler,M., Borazanci,E., McGhee,L., Pylant,S.W., Williams,B.J., Glass,J., Davis,J.N. and Meyers,S. (2006) RUNX1 (AML-1) and RUNX2 (AML-3) cooperate with prostate-derived Ets factor to activate transcription from the PSA upstream regulatory region. *J. Cell. Biochem.*, **97**, 1–17.
42. Huang,H., Yu,M., Akie,T.E., Moran,T.B., Woo,A.J., Tu,N., Waldon,Z., Lin,Y.Y., Steen,H. and Cantor,A.B. (2009) Differentiation-dependent interactions between RUNX-1 and FLI-1 during megakaryocyte development. *Mol. Cell. Biol.*, **29**, 4103–4115.
43. Huang,D.W., Sherman,B.T. and Lempicki,R.A. (2008) Systematic and integrative analysis of large gene lists using DAVID bioinformatics resources. *Nat. Protoc.*, **4**, 44–57.
44. Stenmark,H. and Olkkonen,V.M. (2001) The Rab GTPase family. *Genome Biol.*, **2**, REVIEWS3007.3001-3007.
45. McPherson,P.S. (2010) Proteomic analysis of clathrin-coated vesicles. *Proteomics*, **10**, 4025–4039.
46. Shindou,H. and Shimizu,T. (2009) Acyl-CoA:Lysophospholipid acyltransferases. *J. Biol. Chem.*, **284**, 1–5.
47. Shindou,H., Eto,M., Morimoto,R. and Shimizu,T. (2009) Identification of membrane O-acyltransferase family motifs. *Biochem. Biophys. Res. Commun.*, **383**, 320–325.
48. Wang,Y., Kuhajda,F.P., Li,J.N., Pizer,E.S., Han,W.F., Sokoll,L.J. and Chan,D.W. (2001) Fatty acid synthase (FAS) expression in human breast cancer cell culture supernatants and in breast cancer patients. *Cancer Lett.*, **167**, 99–104.
49. Rossi,S., Graner,E., Febbo,P., Weinstein,L., Bhattacharya,N., Onody,T., Bubley,G., Balk,S. and Loda,M. (2003) Fatty acid synthase expression defines distinct molecular signatures in prostate cancer. *Mol. Cancer Res.*, **1**, 707–715.
50. Wang,Y.Y., Kuhajda,F.P., Li,J., Finch,T.T., Cheng,P., Koh,C., Li,T., Sokoll,L.J. and Chan,D.W. (2004) Fatty acid synthase as a tumor marker: its extracellular expression in human breast cancer. *J. Exp. Ther. Oncol.*, **4**, 101–110.

51. Jourquin,J., Tripathi,M., Guess,C., Quaranta,V., Zent,R. and Pozzi,A. (2010) *Cell-Extracellular Matrix Interactions in Cancer*. Springer, New York, pp. 87–109.
52. Pratap,J., Lian,J., Javed,A., Barnes,G., van Wijnen,A., Stein,J. and Stein,G. (2006) Regulatory roles of Runx2 in metastatic tumor and cancer cell interactions with bone. *Cancer Metastasis Rev.*, **25**, 589–600.
53. Shang,Y., Hu,X., DiRenzo,J., Lazar,M.A. and Brown,M. (2000) Cofactor dynamics and sufficiency in estrogen receptor-regulated transcription. *Cell*, **103**, 843–852.
54. Métivier,R., Penot,G., Hübner,M.R., Reid,G., Brand,H., Koš,M. and Gannon,F. (2003) Estrogen receptor-α directs ordered, cyclical, and combinatorial recruitment of cofactors on a natural target promoter. *Cell*, **115**, 751–763.
55. Nishiyama,A., Xin,L., Sharov,A.A., Thomas,M., Mowrer,G., Meyers,E., Piao,Y., Mehta,S., Yee,S., Nakatake,Y. *et al.* (2009) Uncovering early response of gene regulatory networks in ESCs by systematic induction of transcription factors. *Cell Stem Cell*, **5**, 420–433.
56. Ma,Z., Swigut,T., Valouev,A., Rada-Iglesias,A. and Wysocka,J. (2011) Sequence-specific regulator Prdm14 safeguards mouse ESCs from entering extraembryonic endoderm fates. *Nat. Struct. Mol. Biol.*, **18**, 120–127.
57. Iyengar,S., Ivanov,A.V., Jin,V.X., Rauscher,F.J. III and Farnham,P.J. (2011) Functional analysis of KAP1 genomic recruitment. *Mol. Cell. Biol.*, **31**, 1833–1847.
58. Cai,L., Sutter,B.M., Li,B. and Tu,B.P. (2011) Acetyl-CoA induces cell growth and proliferation by promoting the acetylation of histones at growth genes. *Mol. Cell*, **42**, 426–437.
59. Brar,P.K., Dalkin,B.L., Weyer,C., Sallam,K., Virtanen,I. and Nagle,R.B. (2003) Laminin alpha-1, alpha-3, and alpha-5 chain expression in human prepubetal benign prostate glands and adult benign and malignant prostate glands. *Prostate*, **55**, 65–70.
60. Chia,J., Kusuma,N., Anderson,R., Parker,B., Bidwell,B., Zamurs,L., Nice,E. and Pouliot,N. (2007) Evidence for a role of tumor-derived laminin-511 in the metastatic progression of breast cancer. *Am. J. Pathol.*, **170**, 2135–2148.
61. King,T.E., Pawar,S.C., Majuta,L., Sroka,I.C., Wynn,D., Demetriou,M.C., Nagle,R.B., Porreca,F. and Cress,A.E. (2008) The role of alpha 6 integrin in prostate cancer migration and bone pain in a novel Xenograft model. *PLoS ONE*, **3**, e3535.
62. Oikawa,Y., Hansson,J., Sasaki,T., Rousselle,P., Domogatskaya,A., Rodin,S., Tryggvason,K. and Patarroyo,M. (2011) Melanoma cells produce multiple laminin isoforms and strongly migrate on α5 laminin(s) via several integrin receptors. *Exp. Cell Res.*, **317**, 1119–1133.
63. Kusuma,N., Denoyer,D., Eble,J.A., Redvers,R.P., Parker,B.S., Pelzer,R., Anderson,R.L. and Pouliot,N. (2012) Integrin-dependent response to laminin-511 regulates breast tumor cell invasion and metastasis. *Int. J. Cancer*, **130**, 555–66.